

Title	Multi-function acousto-optic signal processor
Authors	Riza, Nabeel A.
Publication date	1998-08-25
Original Citation	Riza, N. A. (1998) 'Multi-function acousto-optic signal processor', Proceedings of SPIE, 3388, Advances in Optical Information Processing VIII, Aerospace/Defense Sensing and Controls, Orlando, Florida, United States. doi: 10.1117/12.319411
Type of publication	Conference item
Link to publisher's version	10.1117/12.319411
Rights	© 1998 Society of Photo-Optical Instrumentation Engineers (SPIE). One print or electronic copy may be made for personal use only. Systematic reproduction and distribution, duplication of any material in this paper for a fee or for commercial purposes, or modification of the content of the paper are prohibited.
Download date	2023-12-05 03:16:18
Item downloaded from	https://hdl.handle.net/10468/10176



UCC

University College Cork, Ireland
 Coláiste na hOllscoile Corcaigh

PROCEEDINGS OF SPIE

[SPIDigitalLibrary.org/conference-proceedings-of-spie](https://spiedigitallibrary.org/conference-proceedings-of-spie)

Multifunction acousto-optic signal processor

Riza, Nabeel

Nabeel A. Riza, "Multifunction acousto-optic signal processor," Proc. SPIE 3388, Advances in Optical Information Processing VIII, (25 August 1998); doi: 10.1117/12.319411

SPIE.

Event: Aerospace/Defense Sensing and Controls, 1998, Orlando, FL, United States

Multi-function Acousto-optic Signal Processor

Nabeel A. Riza

Center for Research and Education in Optics and Lasers (CREOL)
and the Department of Electrical and Computer Engineering,
University of Central Florida,

ABSTRACT

A novel two dimensional acousto-optic processor is introduced for a variety of two dimensional signal processing tasks that include ambiguity function and range-doppler processing, two dimensional raster format high resolution signal spectrum analysis, and triple correlation function generation. The optical design is based on an optically efficient, in-line, high stability, two dimensional interferometer using four acousto-optic devices. Via the simple technique of Bragg cell carrier offset adjustments, the processor can generate the desired interferometric output on a chosen spatial carrier that is required for bias removal and electronic post-processing. The processor has bandwidth limitations based on the type of Bragg cells used in the system.

1. INTRODUCTION

Since the mid 1970's, various acousto-optic (AO) processors have been proposed for a variety of two dimensional (2-D) signal processing operations [1-14]. These processing operations include ambiguity functions, triple correlations, raster format signal spectrum analysis, and range-doppler processing. Acousto-optic devices (AODs) in parallel 2-D optical architectures were employed in these systems as AODs have the potential to deliver real-time, wide bandwidth, processing capabilities required in high performance radar and communication systems.

Early work concentrated on using the Mach-Zehnder interferometer to form coherent high dynamic range processors such as the triple product operation systems [4]. Because of the inherent mechanical instability and sensitivity of the coherent Mach-Zehnder design, an incoherent-light in-line architecture was proposed for this triple product operation [2]. Although this design was mechanically stable, it suffered from bandwidth and dynamic range limitations, in addition to the fact that only real (non-complex) signals could be processed. Later, modifications to this in-line design included replacing the incoherent light emitting diode (LED) by a coherent source that reduced the bandwidth limitations, although, this led to severe mechanical stability requirements as a high spatial frequency hologram was used in the system [9]. Another high mechanical stability in-line coherent triple product system was proposed, but this was at the expense of loss of input signal processing generality as two signals in the triple product had to be the same [10]. This loss of generality was somewhat recovered by using multiplexing schemes, although at the cost of signal processing bandwidth. Recently, another 2-D AO processor design has been proposed; this one for range-doppler processing [11]. This system uses an in-line interferometric design based on Koster prisms, two crossed Bragg cells, and an intensity modulated laser. Although this design has improved features such as wide bandwidth and sufficient mechanical stability, it too has certain limitations. Because several independent components (e.g., cylindrical lenses, wedge plates) are used in the two separate arms of the interferometer, there is a greater risk of mechanically induced optical instabilities. Furthermore, because the laser is intensity modulated by a product of various diverse bandwidth signals (e.g., reference coded waveform and chirp signal), the desired output term is accompanied by other undesired terms (e.g., chirp factor, several low frequency and dc bias terms) that complicates the electronic post-processing, eventually resulting in an approximate version of the desired function with a limited processor dynamic range. More recently, a hybrid approach to wideband signal range-doppler processing has been proposed that combines the strengths of analog acousto-optics and digital electronics [12]. Another recent method uses both a high frequency wideband architecture and a low frequency narrowband architecture to identify strong narrowband interference signals [13-14].

CREOL/UCF, 4000 Central Florida Boulevard, P. O. Box 162700, Rm 280, Orlando, FL 32816-2700, Tel: 407-823-6829; Fax: 407-823-3354, email: riza@creol.ucf.edu.

The purpose of this paper is to introduce a novel in-line coherent four-product AO processor that can be used for a wide variety of 2-D signal processing tasks. This processor provides several simultaneous features (e.g., mechanical stability, processing generality, high dynamic range capability, ease in bias removal, and complex signal input ports), that were to certain degrees limited in previous architectures. The design is based on the mechanically stable in-line 2-D AO interferometer demonstrated previously for 2-D scanning beam control for microwave phased array antennas [15-16]. The stable interferometric nature of the system with four independent complex signal input ports results in the output desired term having a minimum number of undesired bias terms, leading to a high dynamic range design. Furthermore, the desired output term can be generated on a spatial carrier of any desired frequency and direction by simply changing the carrier frequencies driving the four Bragg cells; thus facilitating bias subtraction and post-processing procedures without requiring additional beam deflecting optics in the system. The AO processor makes efficient use of the input laser light, thus alleviating to some extent, the inefficiency in the double diffraction-cascade nature of the design. This paper first introduces the mathematical foundation behind the four product processor, explaining what conditions are required for the desired four-product output function production and required spatial carrier generation. Next, we describe the input signal conditions for implementing various signal processing functions such as ambiguity surfaces (both for continuous wave (CW) signals/radar and pulse-doppler radar), 2-D raster format real-time signal spectrum analysis with coarse-fine analysis, and triple product correlation processing. The various system features and limitations of the processor are highlighted, including the bandwidth limitation based on the type of the Bragg cells used in the system. Finally, extensions of the 2-D time integrating processor to space-space and space-time processing are also highlighted, alongwith other possible application areas for this 2-D AO processor.

2. TWO DIMENSIONAL ACOUSTO-OPTIC FOUR PRODUCT PROCESSOR - SYSTEMS THEORY

Fig.1 shows a three dimensional view of the proposed 2-D AO processor. Expanded and collimated light from a coherent high power light source such as a 500 mW diode-pumped frequency doubled 532 nm Nd:YAG solid state laser is focussed using cylindrical lens C_{1y} as a Bragg matched slit along the x -direction in AOD1. The Bragg cell AOD1 is driven by a signal $s_1(t)$ riding on a carrier of angular frequency $\omega_c + \delta\omega_1$. Similarly, the other Bragg cells AOD2, AOD3, and AOD4, are driven by their respective signals on their chosen carrier frequencies. Note that the signal modulation driving the AODs can be double sideband amplitude modulation (DSB-AM) where a real signal $s_1(t)$ is mixed with the AOD1 carrier, or single sideband (SSB) amplitude/frequency modulation where only one complex sideband modulation of the input signal rides on the AOD1 carrier. SSB modulation is typically used when complex signal representation and processing is required via the optical processor.

Fig.2 shows the detailed top and side views of the proposed 2-D AO processor. AOD1 generates a +1 order positive doppler shifted, spatially deflected beam in the x -direction that we label as $+1^x$, while the undiffracted DC beam from AOD1 is labelled as DC. The spherical lens S1 takes the $+1^x$ diffracted and dc beams and forms vertical Bragg matched light slits (along the y -direction) in AOD3 and AOD4, respectively. The $+1^x$ beam from AOD1 generates a negative doppler -1^y diffracted beam along the y -direction from AOD3. This double diffracted beam (from AOD1 and AOD3) is called $+1^x, -1^y$. The DC beam from AOD1 generates a positive doppler shifted, y -direction deflected, diffracted beam from AOD4 labelled $+1^y$. This $+1^y$ beam is Bragg matched to AOD2 (in the x -direction), and generates a negative doppler shifted -1^x diffracted beam along the x -direction. This double diffracted beam (from AOD4 and AOD2) is called $-1^x, +1^y$, and it passes through the series of cylindrical lenses C_{1x} , C_{2y} , and C_{2x} to be incident on the 2-D time integrating detector array. The $+1^x, -1^y$ double diffraction beam from AOD1 and AOD3 Bragg diffractions passes through AOD2 essentially uneffected. This beam then also passes through the series of cylindrical lenses C_{1x} , C_{2y} , and C_{2x} to be incident on the 2-D detector array. Thus, the two doubly diffracted beams $+1^x, -1^y$ and $-1^x, +1^y$ interfere on the detector plane with orthogonal coordinates x and y . Note that the DC block spatial filter prevents the undiffracted light beam from hitting the detector array. Note that the spherical lens pair S1 and S2 forms a 1:1 imaging system in x, y between the AOD1 plane and the AOD2 plane, thus maintaining Bragg matching conditions. The cylindrical lens pair lenses C_{1x} , C_{2x} forms a $1:M_x$ imaging system along the x -direction between the AOD2 acoustic axis and the detector plane x -axis. M_x is the magnification factor given by the ratio of the C_{2x} cylinder focal length to the C_{1x} cylinder focal length. Similarly, the sphere S2 and cylindrical lens lenses C_{2y} forms a $1:M_y$ imaging system along the y -direction between the AOD3/AOD4 acoustic axis and the detector plane y -axis. Here M_y is the magnification factor given by the ratio of the C_{2y} cylinder focal length to the S2 sphere focal length. Thus, eventually, the signals fed to AOD1 and AOD2 appear as counter-propagating signals along the x -direction of the 2-D detector, while the signals fed to AOD3 and AOD4 appear as counter-propagating signals along the y -direction of the 2-D detector. This eventually leads to the four-product operation between the four signals fed to the four AODs. Note that there are slight relative deflection angles $\Delta\theta_x$ and $\Delta\theta_y$ along the x and y directions, respectively, between the two interfering beams on the detector array. These deflection angles are

generated through AOD carrier offset frequencies, and are used to generate a desired spatial carrier on the detector plane for bias removal and signal post-processing.

In general, each signal $s_n(t)$, where $n=1,2,3$, and 4, corresponding to AOD1, AOD2, AOD3, and AOD4 drive signals, respectively, are frequency modulated by a particular AOD carrier frequency $\omega_c + \delta\omega_n$, where again “n” is the Bragg cell number. The $\delta\omega_n$ offset AOD carriers are responsible for generating the desired spatial carriers at the output of the processor for bias removal and complex signal domain processing. As an example to highlight temporal and spatial modulations introduced by a Bragg cell, consider a Bragg cell driven only by the particular AOD carrier signal that can be expressed as:

$$s(t) = 2a \cos(\omega_c t + \delta\omega_n t), \quad (1)$$

where “a” is a constant amplitude term, ω_c is the AOD carrier, and $\delta\omega_n$ is the carrier offset signal frequency. In this case, the +1 Bragg diffracted order optical field representation for an acoustic signal travelling in the x-direction can be written as:

$$\tilde{s}(t - x/v) \exp[+j2\pi(\sin\theta_B/\lambda)x], \quad (2)$$

where the carrier-based Bragg angle spatial frequency $2\pi(\sin\theta_B/\lambda) = \omega_c/2v$; v is the AOD signal acoustic signal velocity. Here, the +1 order diffracted signal has a single sideband representation given by:

$$\tilde{s}(t - x/v) = a \exp[-j(\omega_c + \delta\omega_n)(t - x/v)]. \quad (3)$$

Similarly, the -1 Bragg diffracted order optical field representation for an acoustic signal travelling in the x-direction can be written as:

$$\tilde{s}'(t - x/v) \exp[-j2\pi(\sin\theta_B/\lambda)x], \quad (4)$$

where in this case the -1 order signal also has a single sideband representation given by:

$$\tilde{s}'(t - x/v) = a \exp[+j(\omega_c + \delta\omega_n)(t - x/v)]. \quad (5)$$

Note that the “ \sim ” implies a Bragg diffracted signal representation while the presence of a “ $'$ ” implies a -1 order diffraction. Given that AOD1, AOD2, AOD3, and AOD4 are driven by general signals $s_n(t)$ modulated on a $\omega_c + \delta\omega_n$ temporal carrier, we can use the specific Bragg diffracted representations $\tilde{s}_1(t)$, $\tilde{s}_2'(t)$, $\tilde{s}_3'(t)$, and $\tilde{s}_4(t)$, for the AO processor. Thus, the light intensity at the output detector plane can be expressed as:

$$\begin{aligned} I(x, y) &= |A \bullet B + C \bullet D|^2 \\ A &= \tilde{s}_1(t - x/v) \exp[-j(\omega_{cx} + \delta\omega_1)t] \exp[+j(\delta\omega_1/v)x] \exp[+j2\pi(\sin\theta_{Bx}/\lambda)x], +1^x \text{ order AOD1,} \\ B &= \tilde{s}_3'(t - y/v) \exp[+j(\omega_{cy} + \delta\omega_3)t] \exp[-j(\delta\omega_3/v)y] \exp[-j2\pi(\sin\theta_{By}/\lambda)y], -1^y \text{ order AOD3,} \\ C &= \tilde{s}_2'(t + x/v) \exp[+j(\omega_{cx} + \delta\omega_2)t] \exp[+j(\delta\omega_2/v)x] \exp[+j2\pi(\sin\theta_{Bx}/\lambda)x], -1^x \text{ order AOD2,} \\ D &= \tilde{s}_4(t + y/v) \exp[-j(\omega_{cy} + \delta\omega_4)t] \exp[-j(\delta\omega_4/v)y] \exp[-j2\pi(\sin\theta_{By}/\lambda)y], +1^y \text{ order AOD4,} \end{aligned} \quad (6)$$

where ω_{cy} and θ_{By} are the AOD3, AOD4 y-direction Bragg cell pair carrier frequency and Bragg angle, respectively. Similarly, ω_{cx} and θ_{Bx} are the AOD1, AOD2 x-direction Bragg cell pair carrier frequency and Bragg angle, respectively. A, B, C, and D represent the optical field modulations imposed by the Bragg diffractions in the four Bragg cells labelled AOD1, AOD3, AOD2, and AOD4, respectively. The total bias terms can be written as:

$$\begin{aligned} \text{Bias } E &= |A \bullet B|^2 + |C \bullet D|^2 \\ &= |\tilde{s}_1(t - x/v) \bullet \tilde{s}_3'(t - y/v)|^2 + |\tilde{s}_2'(t + x/v) \bullet \tilde{s}_4(t + y/v)|^2. \end{aligned} \quad (7)$$

The desired interferometric term ``F'' can be written as:

$$\begin{aligned}
F &= 2 \operatorname{Re} \left\{ (A \bullet B)^* (C \bullet D) \right\} \\
&= 2 \operatorname{Re} \left\{ \left[\tilde{s}_1^*(t-x/v) \tilde{s}_2'(t+x/v) \tilde{s}_3'^*(t-y/v) \tilde{s}_4(t+y/v) \right] \right. \\
&\quad \bullet \exp \left\{ +j \left[(\partial\omega_1 + \partial\omega_2) - (\partial\omega_3 + \partial\omega_4) + 2(\omega_{cx} - \omega_{cy}) \right] t \right\} \\
&\quad \bullet \exp \left\{ -j \left[(\partial\omega_1 - \partial\omega_2)/v \right] x \right\} \\
&\quad \left. \bullet \exp \left\{ -j \left[(\partial\omega_4 - \partial\omega_3)/v \right] y \right\} \right\}.
\end{aligned} \tag{8}$$

Notice that the interferometric term has four distinct parts. The first part is a product of the four input Bragg diffracted signals. The second part is the exponential representing a temporal modulation. The third and fourth parts represent spatial carriers in the x and y directions, respectively. These spatial carriers are important because they can be used for separating the bias E (which is not on a spatial carrier), from the desired interferometric four-product output term, and for complex-valued signal recovery. As can be observed from Eqn.8, in order to have no temporal variation of the light pattern, which is generally the desired scenario, as when coherently integrating charge via 2-D starring mode charge coupled device (CCD) for coherent optical processing, the condition,

$$2(\omega_{cx} - \omega_{cy}) = (\partial\omega_3 + \partial\omega_4) - (\partial\omega_1 + \partial\omega_2), \tag{9}$$

must be satisfied by tuning the AOD carriers. Furthermore, in some cases, a spatial carrier may not be required at the output plane. In this case, the following conditions

$$\partial\omega_1 = \partial\omega_2 \text{ and } \partial\omega_3 = \partial\omega_4, \tag{10}$$

must also be satisfied by tuning the AOD carriers. Thus, in order to meet both conditions as listed in Eqns. 9 and 10, the following condition, that is,

$$\omega_{cx} - \omega_{cy} = \partial\omega_3 - \partial\omega_1 = \partial\omega_4 - \partial\omega_2, \tag{11}$$

must be met by the processor. Nevertheless, as mentioned before, in most applications, it is desired that the interferometric term be generated on a spatial carrier so that bias can easily be removed via electronic filtering. In this case, Eqn.9 must be satisfied but at least one of the equations in (10) must not be satisfied. There are three scenarios for this condition.

(a) Carrier only in ``x'':

In this case, we need to have $\partial\omega_1 \neq \partial\omega_2$, $\partial\omega_3 = \partial\omega_4$, and $2(\omega_{cx} - \omega_{cy}) = 2\partial\omega_3 - (\partial\omega_1 + \partial\omega_2)$. For example, we can use tellurium dioxide slow shear wave Bragg cells with $f_c = 80$ Mhz and $v = 0.617$ mm/ μ s, where we are using the relation $\omega_{cx} = \omega_{cy} = \omega = 2\pi f_c$. A typical set of carrier offsets is $f_1 = 1$ Mhz, $f_2 = 9$ Mhz, $f_3 = 5$ Mhz and $f_4 = 5$ Mhz. In this case, we get a $(f_2 - f_1)/v = 13$ lines/mm spatial carrier in the x direction along the output CCD.

(b) Carrier only in ``y'':

This is similar to the case in (a), except, here we need to have $\partial\omega_3 \neq \partial\omega_4$, $\partial\omega_1 = \partial\omega_2$, and $2(\omega_{cx} - \omega_{cy}) = (\partial\omega_3 + \partial\omega_4) - 2\partial\omega_1$. For example, we can use gallium phosphide Bragg cells with $f_c = 1$ Ghz ($\omega_{cx} = \omega_{cy}$) and $v = 6.32$ mm/ μ s. A typical set of carrier offsets is $f_1 = 25$ Mhz, $f_2 = 25$ Mhz, $f_3 = 1$ Mhz and $f_4 = 49$ Mhz. In this case, we get a $(f_4 - f_3)/v = 7.6$ lines/mm spatial carrier in the y direction along the output CCD.

(c) Carriers in ``x'' and ``y'':

In this case, we need to have $\partial\omega_1 \neq \partial\omega_2$, $\partial\omega_3 \neq \partial\omega_4$, and $2(\omega_{cx} - \omega_{cy}) = (\partial\omega_3 + \partial\omega_4) - (\partial\omega_1 + \partial\omega_2)$. For example, we can use gallium phosphide Bragg cells with $f_c=1$ Ghz ($\omega_{cx} = \omega_{cy}$) and $v = 6.32$ mm/ μ s. A typical set of carrier offsets is $f_1 = 5$ MHz, $f_2 = 45$ Mhz, $f_3 = 1$ Mhz and $f_4 = 49$ Mhz. In this case, we get a $(f_2 - f_1)/v = 6.33$ lines/mm spatial carrier in the x direction and a $(f_4 - f_3)/v = 7.6$ lines/mm spatial carrier in the y direction along the output CCD. Thus, simply by electronically changing the offset carriers to the AODs, this AO processor allows the generation of output spatial carriers used for bias removal and post-processing.

Note in general that spatial carrier generation can also be implemented or enhanced in the more traditional way by placing properly designed wedge plates in the processor. This approach could some what reduce the design constraints on the Bragg cells, particularly in terms of bandwidth, although at the risk of increasing mechanical stability issues.

3. THE 2-D AO PROCESSOR TWO DIMENSIONAL SIGNAL PROCESSING APPLICATIONS

The following section deals with the various 2-D signal processing applications possible with the proposed AO signal processor.

3.1 Ambiguity Function Processing

Ambiguity function generation is useful in applications where signals are in a dynamic environment, such as when the received signal can have unknown doppler shifts and time delays with respect to a transmitted signal. Two key applications for ambiguity function processing are synchronization of pseudorandom sequences in communication receivers and radar target range and velocity determination. The cross-ambiguity function shown in its symmetric form for signals $r(t)$ and $s(t)$ is defined as

$$A(\tau, f_d) = \int_{-\infty}^{+\infty} s(t + \tau/2) r^*(t - \tau/2) \exp(-j2\pi f_d t) dt, \quad (12)$$

where τ is the time delay and f_d is the Doppler shift between the two signals.

Consider the case when the signals driving the AODs are:

$$\begin{aligned} s_1(t) &= r(t) \cos[(\omega_c + \partial\omega_1)t] & \Rightarrow & \tilde{s}_1^*(t - x/v) = r^*(t - x/v) \\ s_2(t) &= s(t) \cos[(\omega_c + \partial\omega_2)t] & \Rightarrow & \tilde{s}_2'(t + x/v) = s'(t + x/v) \\ s_3(t) &= 2a_1 \cos[(\omega_c + \partial\omega_3)t - \pi bt^2] & \Rightarrow & \tilde{s}_3^{*'}(t - y/v) = a_1 \exp[j\pi b(t - y/v)^2] \\ s_4(t) &= 2a_1 \cos[(\omega_c + \partial\omega_4)t + \pi bt^2] & \Rightarrow & \tilde{s}_4(t + y/v) = a_1 \exp[-j\pi b(t + y/v)^2] \end{aligned} \quad (13)$$

Here AOD1 and AOD2 are fed by the reference and signal waveform modulations, respectively. Note that these modulation representations are general waveform representations and depending on the specific application can be real or complex in nature. AOD3 and AOD4 are fed by slow chirp rate down-chirp and up-chirp signals, respectively. The chirp rate is given by $b = (B_{AOD} / T_s)$, where B_{AOD} is the bandwidth of the AOD and T_s is the duration of the chirp. Typically, $T_s = kT_a$, where k is an integer and T_a is the time aperture of the AOD. For all the examples to follow, the offset carriers for the AODs are set such that Eqn.9 is satisfied (i.e., there is no temporal variation of the light intensity), but there are spatial carriers ω_x and ω_y in the x and y directions, respectively, in the output detector plane for bias removal. The output CCD integrates the light pattern for a duration T_d , where $T_d \geq T_s$. The integrated bias term for the ambiguity function processor (using Eqn.7) is:

$$G = \int_0^{T_d} E dt = \int_0^{T_d} \left[|a_1 r^*(t - x/v)|^2 + |a_1 s'(t + x/v)|^2 \right] dt \quad (14)$$

The desired integrated ambiguity function from the processor (using Eqn.8) is given by:

$$Q(x, y) = \int_0^{T_d} F dt = 2|a_1|^2 \operatorname{Re} \left[\exp\{-j(\omega_x x + \omega_y y)\} \int_0^{T_d} s'(t + x/v) r^*(t - x/v) \exp\{-j2\pi(2by/v)t\} dt \right] \quad (15)$$

Comparing equations (12) and (15), one can conclude that the AO processor does indeed generate the ambiguity surface for the two input signals, where in this case, the coordinates of the time delay and doppler frequency format are expressed as $\tau = 2x/v$ and $f_d = 2by/v$, respectively. Thus, the x and y coordinates of the CCD represent the time delay and doppler frequency coordinates, respectively. The desired ambiguity function rides on a spatial carrier that is used for bias removal.

So far, the AO system analysis presented works fine for a CW signal case, such as CW Doppler radar signals. In the case of a pulse-doppler radar where the waveforms used are pulsed in nature, we need to use range gating of the received pulse in order to coherently integrate over several receive pulses, the signal information for a fixed range/time delay bin. This is done by temporally freezing the received signal $s(t)$ in AOD2 by feeding AOD1 with a periodic impulse train of the type $r(t) = \sum_{-\infty}^{+\infty} \delta(t - nT)$, where $1/T$ is the pulse repetition frequency of the radar. Thus, at the time the impulse occurs, the same range resolution elements are always imaged to the same positions/bins on the 2-D detector output plane. In this way, the proposed 2-D AO processor can also be used for pulse-doppler radar applications. In addition, recently we have investigated this range-doppler processor for inverse synthetic aperture radar (ISAR) applications [17].

3.2 Real-time Two Dimensional Spectrum Analysis

AODs can also be used for high resolution spectrum analysis of wide bandwidth signals. The use of the AO technique is powerful because it is possible to produce arbitrarily small frequency resolution with approximately 10^5 resolvable frequencies in real-time. 2-D spectrum analysis of a signal $s(t)$ can be expressed as:

$$S(f_x, f_y) = \int_{-\infty}^{+\infty} s(t) \exp\{-j2\pi(f_x + f_y)t\} dt \quad (16)$$

where the orthogonal output plane temporal frequencies f_x and f_y are functions of the output plane coordinates x and y, respectively, in an optical spectrum analyzer. f_x represents the temporal coarse frequency of the signal, while f_y represents the fine frequency component.

The proposed 2-D AO architecture can also be used to implement real-time 2-D spectrum analysis. In order to accomplish this task, the laser light input to the AO system needs to be directly or externally intensity modulated in a linear fashion by the signal $s(t)$ that needs to be analyzed. The linear intensity modulation of the laser light can be expressed as:

$$I_s = (1 + m s(t)) \quad (17)$$

where the signal appears on a bias level, and "m" is the signal modulation index. The required signals fed to the AODs are a pair of fast chirp signals to AOD1 and AOD2, and a pair of slow chirp signals (like in the ambiguity function processor) to AOD3 and AOD4. These chirp signals driving the AODs are given by:

$$\begin{aligned}
s_1(t) &= 2a_1 \cos[(\omega_c + \partial\omega_1)t + \pi at^2] \Rightarrow \tilde{s}_1^*(t - x/v) = a_1 \exp[j\pi a(t - x/v)^2] \\
s_2(t) &= 2a_1 \cos[(\omega_c + \partial\omega_2)t - \pi at^2] \Rightarrow \tilde{s}_2'(t + x/v) = a_1 \exp[-j\pi a(t + x/v)^2] \\
s_3(t) &= 2a_1 \cos[(\omega_c + \partial\omega_3)t - \pi bt^2] \Rightarrow \tilde{s}_3^*(t - y/v) = a_1 \exp[j\pi b(t - y/v)^2] \\
s_4(t) &= 2a_1 \cos[(\omega_c + \partial\omega_4)t + \pi bt^2] \Rightarrow \tilde{s}_4(t + y/v) = a_1 \exp[-j\pi b(t + y/v)^2] .
\end{aligned} \tag{18}$$

AOD3 and AOD4 are fed by slow chirp rate down-chirp and up-chirp signals, respectively, as described earlier. AOD1 and AOD2 are fed by fast chirp rate up-chirp and down-chirp signals, respectively. The fast chirp rate is given by $a = (B_{AOD}/T_f)$, where B_{AOD} is the bandwidth of AOD1 (and AOD2) and T_f is the duration of the chirp. Typically, $T_f = T_d$. As before, the offset carriers for the AODs are set such that Eqn.9 is satisfied (i.e., there is no temporal variation of the light intensity), but there are spatial carriers ω_x and ω_y in the x and y directions, respectively, in the output detector plane for bias removal. The output CCD integrates the light pattern for a duration T_d , where $T_d \geq T_s$. The integrated bias term for the spectrum analysis processor (using Eqn.7) and considering that the input laser light is intensity modulated by the signal s(t), is given by:

$$G = \int_0^{T_d} E \bullet I_s dt = 2|a_1|^2 \int_0^{T_d} [1 + m s(t)] dt . \tag{19}$$

Thus, the time integrated bias level consists of a fixed bias level and a signal dependent bias level. If the CCD integration time is fairly long such that it integrates several cycles of the lowest frequency in the signal, the signal bias contribution approaches zero, a result expected as the signal has a zero dc level.

Knowing that $1+ms(t)$ is a real signal, i.e., $S(f)=S^*(-f)$, where $S(f)$ is the temporal Fourier transform of the signal, the desired integrated real-time 2-D spectrum analysis function from the processor (using Eqn.8) and considering the intensity modulation of the laser light, comes to be:

$$Q(x, y) = \int_0^{T_d} F \bullet I_s dt = 2|a_1|^4 \operatorname{Re} \left[\exp\{-j(\omega_x x + \omega_y y)\} \int_0^{T_d} [1 + m s(t)] \exp\{-j2\pi[(2ax/v) + (2by/v)]t\} dt \right] . \tag{20}$$

Comparing eqns. (16) and (20), one can conclude that the AO processor does indeed generate the real-time 2-D raster format spectrum for the input signal s(t), where in this case, the output temporal frequency coordinates f_x and f_y are expressed as $f_x = 2ax/v$ and $f_y = 2by/v$. Thus, the x and y coordinates of the CCD represent the coarse and fine frequency coordinates, respectively, of the input signal s(t). Note that the spectrum analysis expression in Eqn.20 also gives a dc level blur spot at the $x=0, y=0$ output coordinates, as the signal to be analyzed has a unity dc level. The desired spectrum function along with the dc blur spot rides on a spatial carrier that is used for in-phase/quadrature processing and separating the bias term G from the desired spectrum.

3.3 Triple Product Processing

The triple correlation function expressed as

$$c(\tau_1, \tau_2) = \int_{-\infty}^{+\infty} s_1(t) s_1(t + \tau_1) s_1(t + \tau_2) dt , \tag{21}$$

is a useful signal processing tool. In fact, the 2-D Fourier transform of the triple correlation function is the auto-bispectrum (when $s_1 = s_2 = s_3$), which is a sensitive method for discriminating unbiased and biased sinusoidal signals. To implement the triple correlation function from our 2-D AO processor, we need the AOD drive signals to be as follows:

$$\begin{aligned}
s_1(t) &= 2a_1 s(t) \cos[(\omega_c + \partial\omega_1)t] & \Rightarrow \tilde{s}_1^*(t - X/2v) &= a_1 s(t - X/2v) \\
s_2(t) &= 2a_1 p(t) \cos[(\omega_c + \partial\omega_2)t] & \Rightarrow \tilde{s}_2^*(t + x/v) &= a_1 p'(t + x/v) \\
s_3(t) &= 2a_1 \cos[(\omega_c + \partial\omega_3)t] & \Rightarrow \tilde{s}_3^*(t - y/v) &= a_1 \\
s_4(t) &= 2a_1 r(t) \cos[(\omega_c + \partial\omega_4)t] & \Rightarrow \tilde{s}_4^*(t + y/v) &= a_1 r(t + y/v) .
\end{aligned} \tag{22}$$

Here, AOD1 acts as a point modulator, where X is the AOD spatial aperture size. In otherwords, AOD1 acts as a point modulator at its aperture center by using a pin-hole aperture/iris positioned at this AOD position. Another alternative is to replace the deflector AOD1 with an acousto-optic modulator (AOM) that is designed specifically to act as a point modulator.

To complete the analysis, let $t_0 = X/2v$. Then, the time integrated bias term is:

$$G = \int_0^{T_d} E dt = \int_0^{T_d} \left[|a_1^2 s(t - t_0) p'(t - x/v)|^2 + |a_1^2 r(t + y/v)|^2 \right] dt . \tag{23}$$

Furthermore, the desired time integrated triple correlation function from the 2-D AO processor can be expressed as:

$$Q(x, y) = \int_0^{T_d} F dt = 2|a_1|^4 \operatorname{Re} \left[\exp\{-j(\omega_x x + \omega_y y)\} \int_0^{T_d} s(t - t_0) p'(t + x/v) r(t + y/v) dt \right] . \tag{24}$$

Note that if we make the substitutions $t' = t - t_0$, $\tau_1 = t_0 + x/v$, and $\tau_2 = t_0 + y/v$, we can rewrite Eqn.24 as:

$$Q(x, y) = 2|a_1|^4 \operatorname{Re} \left[\exp\{-j(\omega_x x + \omega_y y)\} \int_{-t_0}^{T_d - t_0} s(t') p'(t' + \tau_1) r(t' + \tau_2) dt' \right] . \tag{25}$$

Note the similarity between the integrands of equations 20 and 25, indicating the our 2-D AO processor does indeed give the desired triple correlation function.

4. SYSTEM FEATURES AND ISSUES

The proposed AO system is a coherent architecture that is based on a unique four AO cell in-line design that efficiently uses all the input laser light. In otherwords, all the undiffracted light beams are used for further diffraction and signal modulation and only the left over unmodulated beam is blocked. Assuming that the laser has a power of P Watts and all Bragg cells operate with the same η diffraction efficiency, the light incident on the detector is $2P \eta^2(1-\eta)$ Watts. Thus, given that the AODs operate at a low diffraction efficiency of 10% for linear-mode operation, the processor optical efficiency is 1.8 %. Thus, although current-day CCDs are extremely light sensitive devices, a moderately high power laser source (e.g., > 100 mW) must be used with this system to expect low optical and electrical noise output characteristics. Note that because of the in-line, short relative path-difference nature of our optical interferometric processor, broadband high power lasers such as 1 W laser diodes can be used in this system. In otherwords, long coherence length lasers are not required for this processor. Note that all Bragg cells must be operated at low diffraction efficiencies not only to implement linear electrical-to-optical signal modulations, but also to minimize the modulation effects on the undiffracted beams that flow as input beams to latter Bragg cells to implement Bragg diffracted processing operations.

The design and performance of this system is highly dependent on the types of Bragg cells used in the processor [17]. There are two key reasons for this. The Bragg angle of AOD1 coupled with the focal length F_1 of the spherical lens S1 determines the physical separation Δx between the $+1^x$ diffracted beam and the DC beam from AOD1. $\Delta x = (2 F_1 f_c \lambda/v)$ shows that the type of Bragg cell plays a key role in the physical size of the system. The bigger the separation, the easier it is to place two independent Bragg cells representing AOD3 and AOD4. For a typical radio frequency (rf) Bragg cell such as a flint glass cell

using $f_c = 100$ Mhz, $\lambda = 532$ nm, $v = 3.9$ mm/ μ s, and $F_1 = 10$ cm, we get $\Delta x = 2.73$ mm. The closest we can place two Bragg cells is by stacking them together side by side with a tiny air gap between them. This also means that the acoustic height of each Bragg cell used for AOD3 and AOD4 must not exceed Δx . Typical rf Bragg cells have acoustic heights in the range of 1-15 mm with over 50 % signal bandwidths depending on the cell design. For instance, a typical slow shear wave tellurium dioxide Bragg cell fabricated with a phased array input transducer design had a 60 Mhz bandwidth using a 90 Mhz center frequency, and a 50 μ s time aperture with a 1.85 mm acoustic height/total transducer array length [18]. Thus, two such Bragg cells can be used for AOD3 and AOD4, in the optical design mentioned before where $\Delta x = 2.73$ mm. It is desirable to have a low value for F_1 as this makes the processor shorter, in addition to minimizing the spatial Fourier transform of the signal fed to AOD1 that appears across the AOD3 acoustic height. Note that all this spatial Fourier transform light must fall within the acoustic height of AOD3 to be efficiently diffracted. The disadvantage of going to a shorter focal length is that now the DC and $+1^x$ diffracted beams from AOD1 get closer together, and it is harder to independently place two Bragg cells side by side. In order to have the highest possible processing bandwidth, it is critical that all Bragg cells, particularly, AOD3 and AOD2, that fall in the spatial Fourier transform planes of the input signals, have high (> 50 %) fractional bandwidths. Thus, cells like the tellurium dioxide Bragg cell mentioned before must be used in the system.

Note that Bragg angles associated with microwave band Bragg cells are much larger (e.g., 22 degrees instead of 0.2 degrees) than those used for rf Bragg cells. This means that Δx is much larger than in the rf Bragg cell design, and is typically in the range of 0.5-2 cm. Thus, it is easier to physically place the microwave band Bragg cells in the AOD3/AOD4 position. Nevertheless, because of the higher frequency piezoelectric transducer design requiring much lower capacitance, the acoustic height of these wideband Bragg cells is small (e.g., 50-200 μ m) [19]. This means that the spatial Fourier transform generated by the signals from the preceding AODs might not completely diffract through the acoustic height window of the Bragg cell in the Fourier plane. Thus, depending on the Bragg cells being used in the 2-D AO processor, and the focal length of the Fourier transforming lenses S1 and S2, the system can impose restrictions on the maximum processing bandwidth for the AO processor.

One method for improving the processor design in terms of bandwidth and system size is to replace the single channel Bragg cells AOD3 and AOD4 by an independently driven two-channel Bragg cell [17]. In effect, the bulkier single channel AOD3/AOD4 assembly is replaced by a more compact multichannel Bragg cell assembly where the active acoustic heights of the two channels are maximized via proper placement of the two transducers on the opposite ends of the AO crystal. Recent advances in multichannel Bragg cells have shown less than -30 dB optical crosstalk values between adjacent channels that are on 250 μ m centers with a 125 μ m transducer height [20]. These devices had over 50% fractional bandwidths.

An alternate method to improve processing bandwidth is to use frequency up-conversion of the lower frequency high fractional bandwidth waveforms to form high frequency low fractional bandwidth or narrowband waveforms. Because these narrowband waveforms have much smaller spatial Fourier transforms on the active AOD acoustic height apertures than the high fractional bandwidth waveforms, a much higher percentage of the Fourier transformed light is diffracted by the AOD. The AODs required are of the microwave band type with a very high center frequency relative to the waveform signal bandwidth. For instance, the original waveform might be a 60 Mhz bandwidth signal centered on a 90 Mhz carrier. Such signals are typical in certain high performance radar and communication scenarios. By up-conversion and single sideband (SSB) filtering, this high fractional bandwidth signal can be converted to a narrowband 60 Mhz bandwidth signal centered on a 1 Ghz carrier. To do this, we mix the original rf waveform with a 910 Mhz carrier, and filter/block the lower sideband. The upper sideband is the 1 Ghz signal with the 60 Mhz bandwidth. Thus, we replace all the Bragg cells with microwave band cells to implement the high 60 Mhz fractional bandwidth signal processing.

5. EXTENSIONS AND CONCLUSION

So far, the system introduced is a 2-D AO architecture that implements time integrated processing in the two orthogonal x and y coordinates of the output detector. Our proposed architecture can be modified to implement other 2-D processing options such as space-space processing in both orthogonal output coordinates, or even space-time processing at the output detector. The method to achieve these modifications is implemented by correctly introducing a combination of Fourier transform space integrating optics and/or time integrating imaging optics. By virtue of these extended processing capabilities of the proposed AO processor, it is further possible to host a number of other vital signal processing operations. These include but are not limited to the Wigner-Ville distribution generation, the cross bispectrum function, synthetic aperture radar processing, and image processing applications. Note that the Wigner-Ville distribution is the 2-D Fourier transform of the ambiguity function. Similarly, the cross bispectrum is the 2-D Fourier transform of the triple correlation function. Note that we have described one version of our 4-Bragg cell in-line architecture. It is possible to modify this design by choosing different Bragg diffracted orders

(+1 or -1) and Bragg cell drive signals. For instance, compared to the proposed drive conditions where similar signals drive the x-direction AODs and similar signals drive the y-direction AODs, the x and y-direction Bragg cells can be driven such that a 45 degree rotation of output axes occurs that can lead to certain desired features for specific signal processing applications. These and other extensions of the proposed AO processor will be described in future research.

In conclusion, we have introduced and laid the theoretical foundation for a new 2-D AO signal processing architecture that is a powerful 2-D signal processing tool, particularly for real-time processing of radar and communication waveforms. The system efficiently uses the input optical power, and has a stable in-line interferometric design for high dynamic range complex signal processing. Furthermore, using simple frequency offsets in the AOD carriers, it is possible to produce any desired spatial carrier in the output plane so that bias removal can be implemented via electronic filtering. The processor does have its limitations in terms of the useful processing bandwidth, as determined by the type of Bragg cells used in the system. We suggest a frequency upconversion method to improve the processing bandwidth for wideband rf signals. Future work relates to the experimental demonstration of various signal processing functions including adaptive signal processing concepts.

6. REFERENCES

1. R. A. K. Said and D. C. Cooper, "Crosspath real-time optical correlator and ambiguity function processor," *Proc. IEE*, Vol.120, p.423, 1973.
2. P. Kellman, "Time integrating optical processors," *SPIE Proc.*, Vol.154, p.196, 1978.
3. I. J. Abramovitz, N. J. Berg, and M. W. Casseday, "Interferometric surface wave acousto-optic time integrating correlators," *Proc. IEEE Ultrasonic Symp.*, Boston, MA., pp.483-486, Nov., 1980.
4. T. M. Turpin, "Spectrum analysis using optical processing," *Proc. IEEE*, Vol.69, No.1, pp.79-92, Jan., 1981.
5. W. T. Rhodes, "Acousto-optic signal processing: convolution and correlation," *Proc. IEEE*, Vol.69, No.1, p.65, 1981.
6. J. D. Cohen, "Ambiguity processor architectures using one dimensional acousto-optic transducers," *Proc. SPIE*, Vol.180, p.134, 1979.
7. A. W. Lohmann and B. Wirnitzer, "Triple correlations," *Proc. IEEE*, Vol.72, p.889, 1984.
8. A. VanderLugt, "Crossed bragg cell processors," *Appl. Opt.*, Vol.23, p.2275, 1984.
9. M. A. Krainak and D. E. Brown, "Interferometric triple product processor (almost common path)," *Appl. Opt.*, Vol.24, p.1385, 1985.
10. J. D. Cohen, "High bandwidth triple product processor using a shearing interferometer," *Appl. Opt.*, Vol.24, No.19, pp.3173-3178, 1985.
11. L. Harrison, E. Viveiros, M. Patterson, C. Anderson, R. Durrett, N. Mohon, and R. Berinato, "Acousto-optic range Doppler processor for radar insertion," *SPIE Proc.*, Vol.1958, pp.71-82, 1993.
12. K. R. Frampton, et. al., "Acousto-optic range Doppler processor performance," *SPIE Proc.*, Vol.2562-07, July 1995.
13. D. C. Hartup and W. T. Rhodes, "Acousto-optic processor for carrier frequency and envelope modulation analysis," *SPIE Proc.*, Vol.1704, pp.98-104, 1992.
14. B. Tasic and V. M. Ristic, "Triple product optical processor for analysis of pulse-repetition and carrier frequencies of radar signals," *Applied Optics*, Vol.34, No.35, pp.8144-8147, 10 Dec., 1995.
15. N. A. Riza, "Acousto-optic architecture for two dimensional beam scanning in phased array antennas," *Applied Optics*, Vol.31, No.17, pp.3278- 3284, June 10, 1992.
16. N. A. Riza, "Experimental demonstration of an acoustooptic system for two dimensional phased array antenna scanning," *Applied Optics*, Vol. 32, No. 11, pp. 1936-1942, April 10, 1993.
17. N. A. Riza and D. R. Pape, "Photonic signal processing for inverse synthetic aperture radar imaging," *SPIE Proc.*, Vol.3388, No.9, Orlando, April 1998.
18. Photonic Systems Inc., and MVM Electronics, Inc., both in Melbourne, Florida.
19. Acoustooptic Products Catalog, Brimrose Corp. of America, Baltimore, Maryland.
20. D. R. Pape, "Multichannel Bragg cells: design, performance, and applications," *Optical Engineering*, Vol.31, No.10, pp.2148-2158, Oct., 1992.

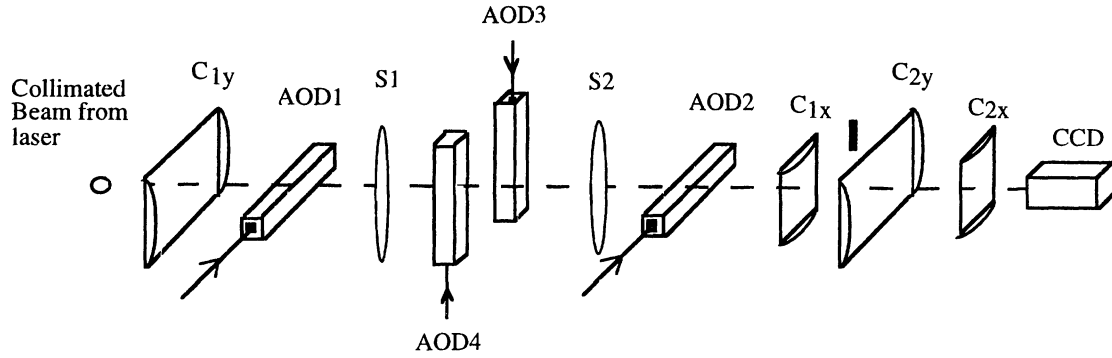


Fig.1 shows a three dimensional view of the proposed four Bragg cell acousto-optic processor for various two dimensional signal processing operations. The processor is shown in its two dimensional time integrating mode.

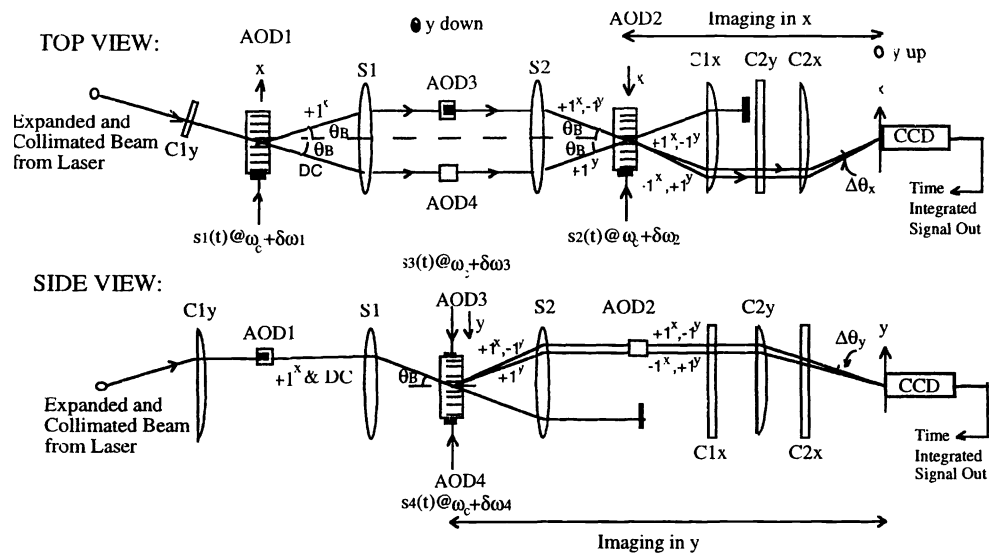


Fig.2 shows the top and side views of the proposed four Bragg cell acousto-optic processor. The figure shows the various Bragg diffracted beams in the system, and the final beam pair that interferes on the 2-D time integrating detector shown here as a CCD.